Capillary Discharge Based Pulsed Plasma Thrusters

IEPC-2007-238

Presented at the 30th International Electric Propulsion Conference, Florence, Italy
September 17-20, 2007

Jean-Luc Cambier*
Air Force Research Lab, 10. E. Saturn Blvd. Edwards AFB, CA 93524, United States

Marcus Young† and Leonid Pekker‡
ERC Inc., 10. E. Saturn Blvd. Edwards AFB, CA 93524, United States

and

Anthony Pancotti§
University of Southern California, 854 W 36th Place, RRB 101, Los Angeles, CA 90089, United States

Abstract: **Although pulsed plasma thrusters have significant experimental heritage over a range of power levels, more recently they are often described as attractive low-power thrusters due to their small dimensions, simplicity, and ability to provide high specific impulses at low power levels. This paper, however, discusses research into the potential application of an electrothermal capillary discharge as a pulsed plasma generator useful in high-power spacecraft propulsion. A 0D transient physical model of the capillary discharge was constructed and used to characterize the operational envelope of the capillary discharge. Fundamental experimental investigations were also conducted to demonstrate the performance of the polyethylene capillary discharge over a range of energy/shot levels (500-1500J), capillary lengths (4cm-10cm), and LRC circuit inductances (10μH-40μH). The experimentally measured parameters (voltage difference, current, ablated mass, plasma temperature, and electron number density) typically agreed with the model predicted values to within 20%. Thruster relevant performance calculations were made using the validated model and showed that even without nozzle expansion the capillary discharge can operate as an efficient (30-40%) source of high-pressure (>100 atm) plasma for use in spacecraft propulsion systems.**

Nomenclature

A	=	averaged atomic mass of the plasma
C	=	capacitance
$C_{s,end}$	=	speed of sound at exit
d	=	capillary diameter
F_{rad}	=	incoming radiation flux to the transition-boundary layer
h_{CH}	=	enthalpy of an outgoing CH-molecule
I	=	applied current
I_{sp}	=	specific impulse
k	=	Boltzmann constant

* Program Manager, AFRL/PRSA, jean-luc.cambier@edwards.af.mil.
† Research Scientist, ERC Inc., Marcus.Young.ctr@edwards.af.mil.
‡ Research Scientist, ERC Inc., Leonid.Pekker.ctr@edwards.af.mil.
§ Ph.D. Student, AME Department, Anthony.Pancotti.ctr@edwards.af.mil.

L = capillary length
M_C = carbon atomic mass
M_H = hydrogen atomic mass
n_{CH} = CH-molecular number density
$n_{CH,end}$ = CH-molecular number density at the open end
N_e = electron number density
R_a = capillary radius
t = time
T = temperature
T_{end} = temperature at the open end
$V_{cap,i}$ = initial capacitor voltage
Z = ionization fraction
$\alpha_{1/2}$ = fractional intensity width
α_C = stoichiometric coefficients of carbon of the molecular wall composition
α_H = stoichiometric coefficients of hydrogen of the molecular wall composition
β = ratio of thermal to magnetic pressure
γ = ratio of specific heats
ΔV = mission velocity increment
$\Delta\lambda_{1/2}$ = full width half max for Stark Lorentzian
ε_{CH} = internal energy of CH-plasma per one CH-molecule
η = power conversion efficiency
λ_{rad} = radiation mean free path
σ = plasma conductivity

I. Introduction

A. Pulsed Plasma Thrusters

Electric propulsion systems have proven advantageous over traditional chemical propulsion systems for several classes of missions such as those with high total velocity increment (ΔV) requirements. A broad range of spacecraft electric propulsion systems have been developed with one class, the pulsed plasma thruster (PPT), using deposited energy from transient electrical pulses to increase the propellant exhaust energy. The pulsed plasma thruster exemplar is a simple and reliable device that ideally employs electromagnetic forces to accelerate decomposition products that have been ablated using a surface discharge on the face of a spring-fed breech-located Teflon® propellant bar. The PPT class, however, is very broad with a range of configurations for gas-fed, liquid-fed, and solid-fed systems which leads to a correspondingly broad range in performance levels.[1]

PPTs are often described as low-power electromagnetic devices, but there has also been steady progress in the development of both high-power PPTs[2] and electrothermal PPTs[3-4]. Figure 1 summarizes the development of both flight and experimental pulsed plasma thrusters in terms of their thrust per unit power and specific impulse, I_{sp}, for a selection of pulsed plasma thrusters described in published literature. There is a classic tradeoff between thrust/power and I_{sp} that is shown by the solid lines in Fig. 1.[5] Each different color corresponds to a different power conversion efficiency (thrust power to input power ratio), η, and illustrates the classic result that increasing the specific impulse, I_{sp}, will decrease the thrust per unit power for a constant η. Figure 1 also indicates that only a small fraction of the experimental PPTs have yet been able to reach a power conversion efficiency of greater than 50%, while flight qualified PPTs (solid blue diamonds) have always operated at efficiencies below 10%. The consistently low power conversion efficiency is the main limitation of pulsed plasma thrusters and is also a main focus of PPT development.

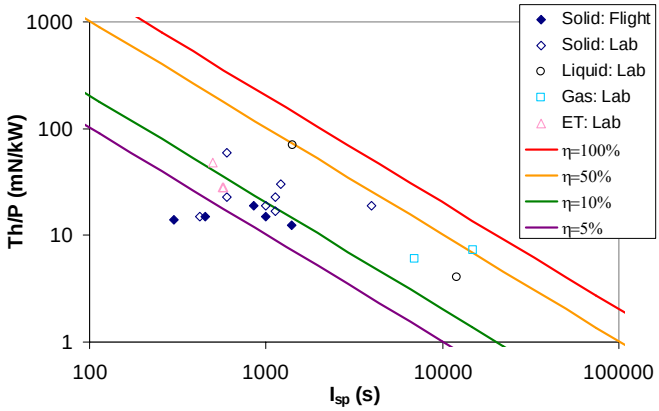

Figure 1. Pulsed Plasma Thruster Development Trends.

From Fig. 1 is appears that flight qualified pulsed plasma thrusters (all solid-fed) have increased in specific impulse and energy conversion efficiency, but stayed relatively constant in thrust per unit power. In general modern flight qualified PPTs have energy conversion efficiencies below 10%, specific impulses around 1000s, and thrust per unit powers of 10-20 mN/kW. A typical example is the PPT designed for the EO-1 spacecraft.[6] Experimental pulsed plasma thrusters achieve a much broader range of performance because they include a wider range of power levels and configuration for solid, liquid, and gas fed versions. Experimental PPTs have operated at I_{sp}s in excess of 10,000s for gas-fed versions and some liquid-fed versions, but solid-fed versions and electrothermal versions are limited to roughly 1000s. Electrothermal or other low I_{sp} designs are often advertised as high thrust devices while high-I_{sp} electromagnetic versions may provide mass savings benefits from operating at higher I_{sp}s. It is clear, however, that increasing the energy conversion efficiency at any I_{sp} would be beneficial. In particular, increasing the energy conversion efficiency of an electrothermal PPT could yield an efficient high thrust/power thruster with an I_{sp} of around 1000s.

B. Capillary Discharge and Coaxial Electrothermal PPT Development

Capillary discharges are efficient sources of high-density ($5x10^{25}$ – $5x10^{26}$ m^{-3}), high-temperature (2–8 eV) pulsed plasmas which are being developed for a wide range of applications including optical guides for high power lasers[7] and x-ray sources[8] for low pressure capillary discharges and electro-thermal-chemical guns[9-13] for high-pressure capillary discharges. Capillary discharges maintain a resistive arc through a narrow insulating capillary by the continual ablation of the capillary wall material or by injected mass. Their high power conversion efficiency (50-70%), high plasma pressure (10^7-10^9 Pa), high-β (>10) and local thermodynamic equilibrium (LTE) conditions also make them a candidate for high-power electrothermal pulsed plasma thrusters.[14]

Figure 2 illustrates the typical capillary discharge geometry. Capillary discharges typically consist of a high-density polyethylene (HDPE) capillary tube, a tungsten anode inserted into one side of the tube, and a cylindrical stainless steel cathode on the outside of the opposite end of the tube. They are typically ignited by shunting current through a fine copper wire strung between the anode and cathode. The wire explodes in several μs and provides the initial plasma used to ignite the main discharge. Two concerns relating to the application of capillary discharges in spacecraft propulsion systems are immediately apparent: the single-use wire ignition system and the lack of a propellant feed mechanism.

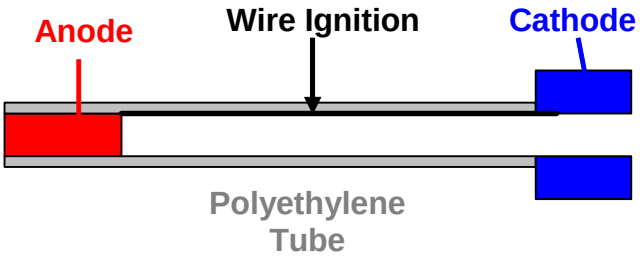

Figure 2. Capillary Discharge Schematic.

Coaxial electrothermal PPTs have been under investigation for decades in both solid-fed[3,4] and liquid-fed[15,16] configurations. In fact, although they are not commonly referred to as such, many coaxial electrothermal PPTs can be considered capillary discharges. One water-fed capillary discharge based propulsion systems encountered difficulties with propellant utilization.[15] Capillary discharge based propulsion systems utilizing liquid hydrogen as propellant have also been analyzed and appeared to be an attractive concept, but may be limited due to difficulties in long-term liquid hydrogen storage.[16] There has been some research into the application of capillary discharge based devices for spacecraft propulsion, but additional investigations are required especially to demonstrate reliable ignition and propellant feeding.

II. Capillary Discharge Model

A. Plasma Model

A zero-dimensional capillary discharge model, Fig. 3, incorporating various radiation models has been developed. The model includes the thermodynamics of partially ionized plasmas, non-ideal high-density plasma effects, and assumes local thermodynamic equilibrium (LTE), fully dissociated plasma, no heat losses into the capillary walls, and a ratio of thermal to magnetic pressure much greater than unity (β>>1).

Introducing the CH-molecular number density, n_{CH}; the internal energy of CH-plasma per one CH-molecule, ε_{CH}; the total enthalpy per CH-molecule in the plasma volume, h_{CH}; assuming sonic conditions at the capillary end, Fig. 3; and taking into account that the plasma is adiabatically outgoing from the capillary end and that the enthalpy of an

outgoing CH-molecule, h_{CH}, is equal to the enthalpy of a CH-molecule in the plasma core (adiabatically-stagnation condition), the equations describing mass and energy conservation laws in the capillary discharge can be written as

$$\pi \cdot R_a^2 \cdot L \cdot \frac{dn_{CH}}{dt} = \frac{F_{rad}(n_{CH},T)}{h_{CH}(n_{CH},T)} - \pi \cdot R_a^2 \cdot n_{CH,end} \cdot C_{s,end}\left(n_{CH,end},T_{end}\right) \quad (1)$$

$$\pi \cdot R_a^2 \cdot L \cdot \frac{d(n_{CH} \cdot \varepsilon_{CH})}{dt} = \frac{I^2 \cdot L}{\pi \cdot R_a^2 \cdot \sigma(n_{CH},T)} - \pi \cdot R_a^2 \cdot n_{CH,end} \cdot C_{s,end}\left(n_{CH,end},T_{end}\right) \cdot h_{CH}\left(n_{CH},T\right) \quad (2)$$

where

$$h_{CH} - \varepsilon_{CH} = kT,\ n_{CH,end} = n_{CH}\left(\frac{2}{\gamma+1}\right)^{1/\gamma-1},\ T_{end} = \left(\frac{2}{\gamma+1}\right)T,\ C_{s,end} = \left[\frac{\gamma kT_{end}\cdot(1+Z)}{AM_H}\right]^{1/2},\ A = \left(\frac{\alpha_C M_C + \alpha_H M_H}{\alpha_C + \alpha_H}\right) \quad (3)$$

Here I(t) is the applied current, σ is the plasma conductivity, A is the averaged atomic mass of the plasma, α_C and α_H are stoichiometric coefficients of carbon and hydrogen of the molecular wall composition. In these expressions, the CH-molecular ablation rate (the total number of CH-molecules ablated per second) is expressed through the incoming radiation flux to the transition-boundary layer $F_{rad}(n_{CH},T)$ and the enthalpy required to bring a single CH-molecule from the capillary wall to the plasma core (no heat losses in the wall). In the model, the transition layer between the wall and the plasma core is assumed to be negligibly thin, Fig. 3, and the radiation flux, $F_{rad}(n_{CH},T)$, and the plasma composition are calculated using PrismSPECT software[17].

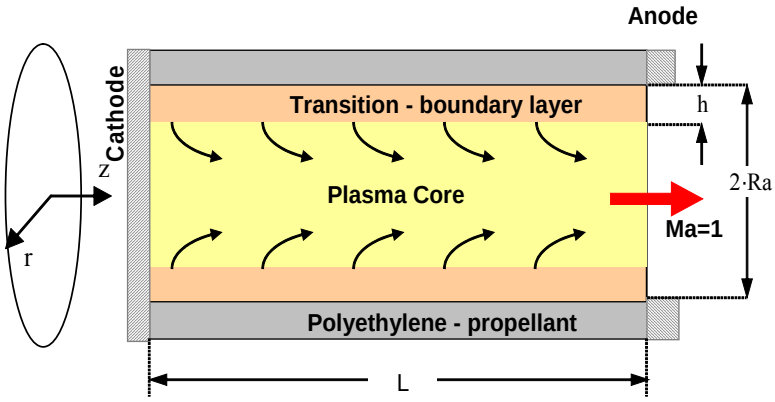

Figure 3. 0D Capillary Discharge Model.

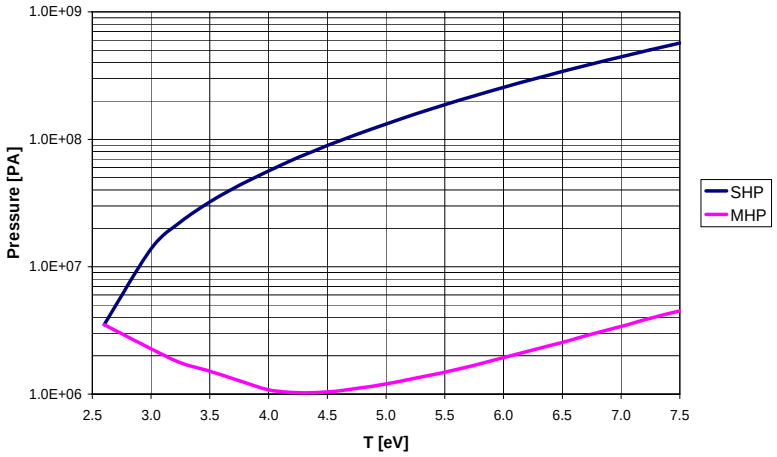

Figure 4. SHP and MHP Regimes for C_4-H_9 Wall Composition. *L = 1cm, R_a = 2mm.*

The models predict the existence of two steady-state regimes of plasma pressure for ablative discharges at a given plasma temperature. The first regime occurs when the plasma is so dense (~10^{26} m^{-3}) that the radiation mean free path, λ_{rad}, is less than the capillary radius, the case of super-high pressure capillary discharge. The second one occurs when the plasma density is much lower (~10^{24} – 10^{25} m^{-3}) such that λ_{rad} is much larger than the capillary radius, i.e. the case of moderate plasma density. As shown in Fig. 4, the regimes converge at small plasma temperature, and there is no steady-state solution for a plasma temperature smaller than 2.6 eV for a 1cm long capillary. The calculations show that with an increase in the capillary length, the density of the plasma in the second regime (where λ_{rad}>>R) becomes so small, that the conduction heat flux to the wall becomes larger than the radiation flux to the capillary wall. In the super-high pressure regime (λ_{rad}~R) the radiation heating of the wall for all capillary lengths is always a few orders of magnitude larger than conduction heating of the wall. Thus, with an increase in the capillary length, the first of the steady-state plasma regimes is always determined by radiation (super-high pressure regime, λ_{rad} ~ R) and the second one (the moderate-pressure regime) transitions from the radiation mode where λ_{rad} >> R to the thermal conduction mode. A rigorous investigation of such a transition

between the radiation and conduction modes cannot be performed by any 0D model and, therefore, is beyond the scope of this paper.

Both regimes may be attractive for thruster applications depending on the specific configuration so both have been investigated in terms of their stability. The evolution of plasma parameters for various ignition number densities and plasma temperature has also been investigated as shown in Fig. 5 and Fig. 6. As on can see the characteristic time scale to achieve steady-state conditions is a few tens of microseconds.

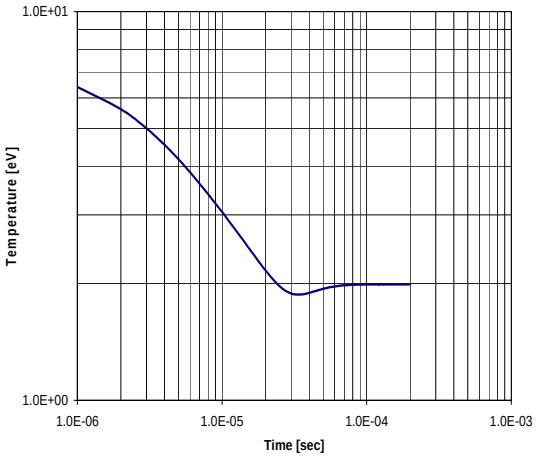

Figure 5. C_4-H_9 Based Capillary Discharge Temperature Evolution.
I = 6.5kA, $T_{steady\text{-}state}$ = 2eV, $n_{steady\text{-}state}$ = 6.8e25 1/m^3, Initial Conditions: T = 7.5eV, n = 5.2e27 1/m^3, R_a = 2mm, L = 5cm.

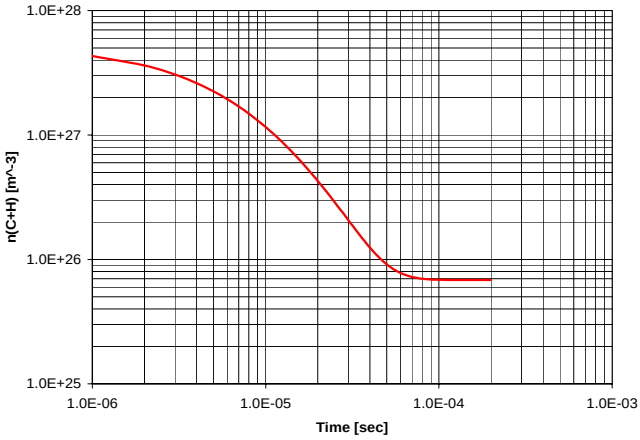

Figure 6. C_4-H_9 Based Capillary Discharge Number Density Evolution.
I = 6.5kA, $T_{steady\text{-}state}$ = 2eV, $n_{steady\text{-}state}$ = 6.8e25 1/m^3, Initial Conditions: T = 7.5eV, n = 5.2e27 1/m^3, R_a = 2mm, L = 5cm.

B. Ignition Model

As indicated earlier the exploding wire ignition system is not practical for satellite propulsion systems. It was, however, chosen for the present work to bridge comparisons with previously published work with future planned experiments with alternative ignition systems. The exploding wire process is very complex and several centuries of investigations have yet to provide a complete understanding of the process.[18] Therefore, no serious attempt was made to accurately model the exploding wire ignition process. A very simple model was created, however, to provide some understanding of its effect on the entire capillary discharge pulse.

Typical maximum resistive input power levels encountered during the exploding wire ignition are on the order of MW, while the maximum radiation cooling power emitted from the ignition wire is on the order of 100W making it negligible. Energy loss through conduction heat transfer along the wire is similarly negligible. For the simple model it is then completely reasonable to neglect all cooling fluxes. It is assumed that the wire has a uniform cross-section that can expand when heated. The model uses the experimentally measured current pulse to calculate the energy deposited in the wire for each timestep based on its temperature dependent resistivity and wire geometry. The temperature is then updated using the relevant specific heat and/or phase change enthalpy. Figure 7 shows the estimated wire temperature compared with the experimentally measured ignition current pulse for a 0.004" diameter, 10cm long aluminum wire and an initial capacitor voltage of 3500V. The temperature rises rapidly as the current pulse increases until about 7μs. At this point the wire has begun to liquefy and the temperature stays constant during liquification while the current begins to decrease. After the wire has fully liquefied the wire temperature increases rapidly until the wire begins to

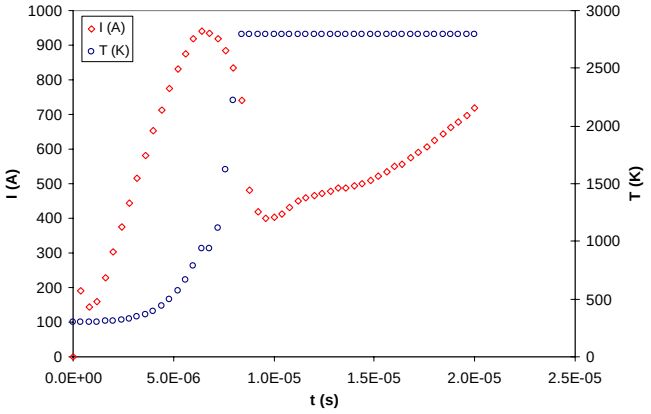

Figure 7. Wire Ignition Temperature Evolution @ 3500V.

vaporize. If sufficient energy is not deposited in the vaporized gas before the wire is fully vaporized the exploding wire will not ignite the main discharge. If the wire blows locally near the anode instead of uniformly a delay between the ignition and the main discharge pulse of up to several hundred microseconds can occur. The transition from the wire explosion to the main capillary discharge pulse is not modeled because of its complexity, but a general understanding of the process and the relevant time-scales was gained with the simple model. A combined LRC circuit/ignition/plasma model was created that uses an equivalent LRC circuit model to first drive the exploding wire ignition and then the main plasma discharge. An assumed plasma number density and temperature are used as initial conditions for the main plasma model once the exploding wire has fully vaporized.

III. Capillary Discharge Experiment

A. Experimental Setup

Capillary discharge experiments were conducted for a variety of geometries, discharge circuit parameters, exploding wire ignition systems, and discharge power levels to gain a basic physical understanding of their operation and to validate the physical model. A cutaway schematic of the main capillary discharge geometry used during the experiments is shown in Fig. 8. The capillary itself is a high-density polyethylene (HDPE) tube with and inner diameter of 4mm. A lanthanated tungsten anode was slid into one side of the HDPE tube. Anodes of different lengths were used during the experiment allowing the capillary length to be effectively varied from 4cm to 10cm. The anode/tube assembly was inserted into the cathode/housing with consisted of two stainless steel weldneck flanges that were welded together. The exploding wire ignition system is simply a 0.004" aluminum wire strung through the capillary and attached to both electrodes.

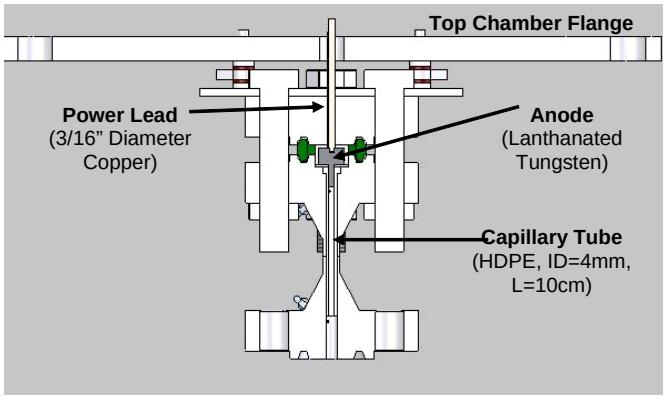

Figure 8. Cutaway Schematic of Capillary Discharge

A schematic showing the capillary discharge experimental setup is shown in Fig. 9. A desktop PC running LabVIEW software and a National Instruments PXI data acquisition (DAQ) system were used for all triggering and data acquisition at a rate of 2.5MHz. A simple LRC circuit was used to drive both the capillary discharge ignition and main discharge circuit. The capacitor bank consisted of four 500 μF, 6 kV General Atomics capacitors (model #32259) although for the results described here only a single capacitor of the bank was used. Four nominally 10μH inductors were also available and were inserted in the circuit in various series/parallel configurations to investigate the effect of the circuit inductance on the operation of the capillary discharge. A high-power Westcode thyristor (model #R3708FC45V), was triggered from the National Instruments DAQ/triggering system to initiate the discharge.

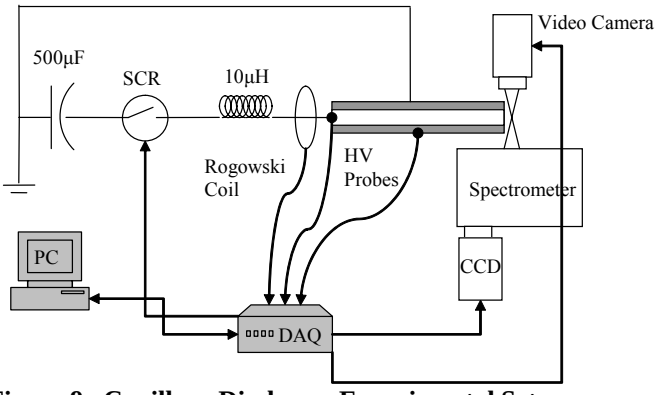

Figure 9. Capillary Discharge Experimental Setup

The diagnostics suite for the capillary discharge experiments consisted of current measurements, voltage measurements, spectroscopic measurements, and high-speed video of the plume. The current measurements were made using Power Electronic Measurements Rogowski coils (model #CWT 600B/2.5/700) both at the connection of the positive output line to the capacitor bank and just before the positive power line connects to the capillary discharge. Voltage measurements were made using Ross Engineering high voltage probes (model #VD45-8.3-A-K-A) at the connection of the positive line to the capacitor bank and at the power lead connection to the capillary discharge. The voltage on the cathode side of the discharge was never more than 200V relative to capacitor ground

and was measured using a simple voltage divider. A Vision Research high-speed video camera (model #v7.3) was also used to image the plume with speeds of up to 100,000 frames per second at an exposure time of 2 μs.

Spectroscopic measurements were taken by collecting light from just outside the cathode exhaust and transporting it to a Princeton Instruments SpectraPro SP-2558 spectrograph using a 10μm diameter silicon fiber optic cable. The spectral image was collected using a Princeton Instrument PIXIS 400 CCD camera. The CCD camera was operated in kinetics mode by illuminating the same 10 pixels and transferring the stored charge up one pixel every 3.2μs providing a temporal resolution of 32 μs.

Discharge measurements were taken for a variety of conditions in order to investigate the basic operation of the capillary discharge and validate the performance model. Table I lists the important experimental parameters for the three sets of capillary discharge tests for various initial capacitor voltages, circuit inductances, and capillary lengths. Each test was repeated a minimum of three times to determine the repeatability of the measurements.

Table I. Experimental Parameters

Initial Capacitor Voltage Tests	Circuit Inductance Tests	Capillary Length Tests
$V_{cap,i}$[V]: 2500,2750,3000,3250,3500 L[cm]: 10 L_{cir} [μH]: 14.4	$V_{cap,i}$[V]: 3000 L[cm]: 10 L_{cir} [μH]: 14.4, 26.1, 40.5, 54.9	$V_{cap,i}$[V]: 2500 L[cm]: 4,5,6,8,10 L_{cir} [μH]: 14.4

B. Circuit Diagnostics

The most easily measured, most accurate, and most repeatable measurements made during the course of this work were the current flowing through the capillary discharge and the voltage difference across the capillary discharge. Both quantities were measured at 0.4μs intervals. Figure 10 illustrates an example of a typical discharge current and voltage trace for the conditions of $V_{cap,i}$ = 2500V, C = 0.55mF, d = 4mm, L = 10cm. The discharge current trace shows a clear double peak structure. The first peak is due to the ignition wire explosion which was discussed earlier. The second peak represents the main discharge. A delay of up to several hundred μs (also the time scale of the main discharge) has been observed between the ignition wire explosion and the main discharge initiation.

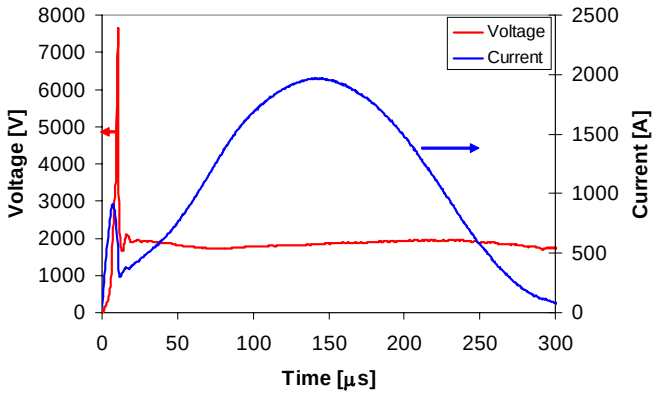

Figure 10. Typical Discharge Voltage and Current Traces.

Figure 11 shows the experimentally measured discharge current traces for five different initial capacitor voltages at the conditions listed in Table 1 and compares them with the model predicted traces. A minimum of three different runs were taken for each condition and all three runs are shown for the 3500V case to show the repeatability of the measurements (typically 10% for peak current and pulse width). There is a clear increase in maximum discharge current with increasing initial capacitor voltage, but the discharge pulse length of the main discharge stays relatively constant at about 250μs. The current traces predicted using an equivalent LRC circuit model and the 0D plasma model are in rough agreement with the experimentally measured values, although several differences are plainly visible. The peak currents agree well at 3000V, but the model tends to under-predict the peak current at higher capacitor voltages and over-predict the peak current at lower capacitor voltages. No attempt was made to accurately model the capillary discharge ignition so a discrepancy at early times is expected, but the discrepancy at late times with the model predicting a long tail extinction that is not seen in the experiments must be further investigated.

Figure 12 shows a similar comparison of discharge current traces verses time for different capillary lengths. Results are only shown for the two extreme lengths for clarity. At shorter capillary lengths higher main discharge peak current levels are achieved primarily because the path length between the electrodes is shorter which reduces the resistance. For capillary lengths less than 10cm, however, two distinct modes of operation were observed. The repeatability of each mode is still better than 10%, but the two different modes can occur for exactly the same nominal conditions. The low-current, longer pulse mode appears to agree reasonably well with the model predictions, but the high-current shorter pulse length mode is clearly a distinct mode. More research into the dual mode is required, but it is clear that the modes are different from the earliest times indicating that the ignition plays a

key role. Figure 13 shows the comparison of the discharge current traces for various numbers of inductors (nominally 10μH) in series and the conditions listed in Table 1. As expected an increase in inductance causes a decrease in the peak current and an increase in the pulse length.

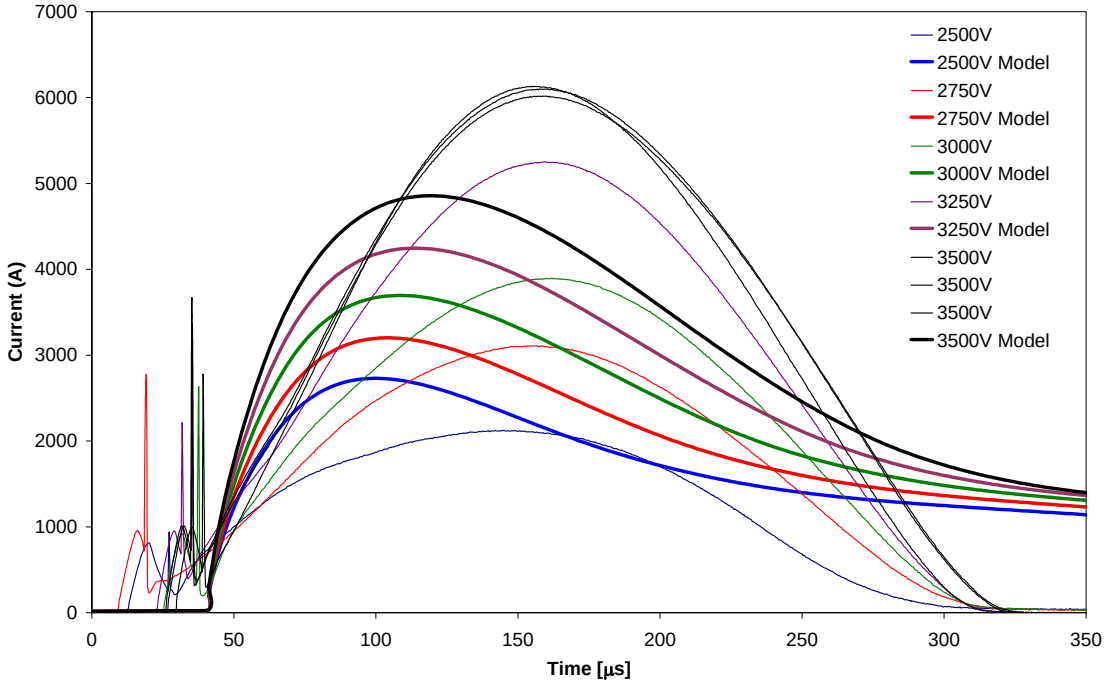

Figure 11. Current Trace Dependence on Initial Capacitor Voltage

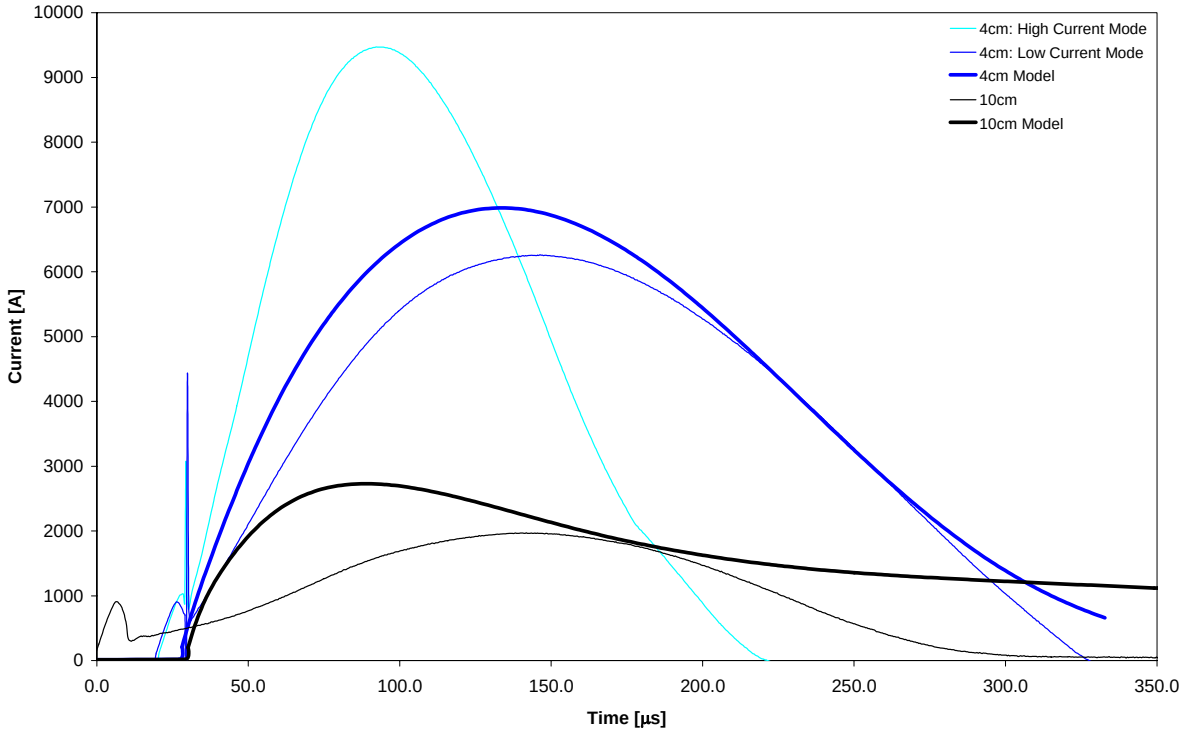

Figure 12. Current Trace Dependence on Capillary Length

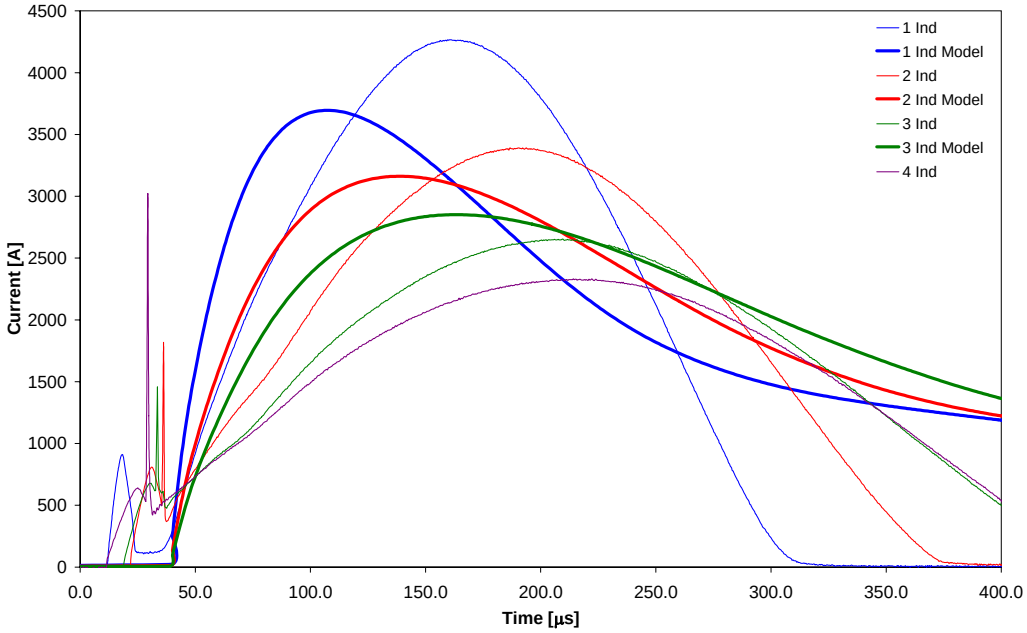

Figure 13. Current Trace Dependence on Circuit Inductance

C. Mass Ablation Measurements

The mass loss of both the polyethylene tube and the lanthanated tungsten anode were measured for each discharge using a Sartorius scale (model #CP224 S) with an uncertainty of 0.1mg. Although the cathodes did show visible surface modification, they did not show measurable mass loss for individual runs. The mass loss for a single pulse as a function of the initial capacitor voltage is shown in Fig. 14. Both the capillary and the anode show measurable mass loss over the entire range of initial capacitor voltages and both increase as the initial capacitor voltage is raised. The anode mass loss increases at a relatively faster rate. Both the experimentally measured capillary mass loss and the model predicted capillary mass loss show the same trends, although the model predicted values are consistently higher. The discrepancy is primarily due to the long tail extinction predicted by the model that is not observed experimentally. Similar agreement is observed for the capillary length and circuit inductance runs.

There are three relevant energies per pulse for this experiment: energy drained from capacitor, energy deposited into the discharge, and kinetic thrust energy. No direct thrust measurements were taken during the experiment so the experimental thrust energy was not determined, but all of the other energies for both the experiment and the model are shown in Fig. 15. As expected the energy levels increase with an increase in the initial capacitor voltage for both the model and the experiment. The model predicted values are consistently higher than the experimentally measured values, although the slopes are similar. The discrepancy is, again, primarily due to the long tail extinction predicted by the model and not observed in the experiments. The model predicted thrust efficiency is relatively

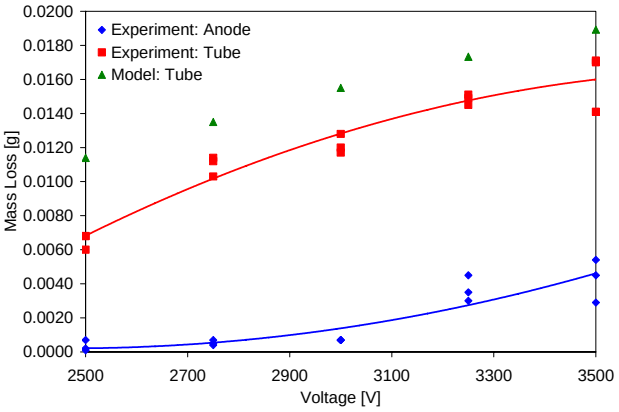

Figure 14. Ablated Mass Verses Initial Capacitor Voltage.

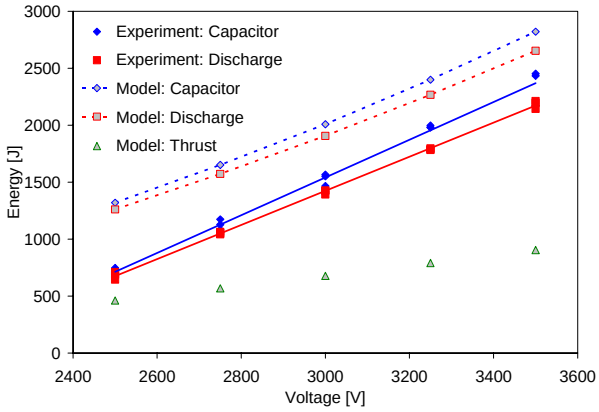

Figure 15. Pulse Energy Verses Initial Capacitor Voltage.

constant for this range of initial capacitor voltages, but is consistently between 30% and 35%.

D. Plasma Temperature and Number Density Measurements

Spectroscopic techniques are commonly used to determine the plasma temperature and electron number density in capillary discharges.[19] The plasma temperature is commonly determined by comparing the relative intensities (Boltzmann plot method) of copper lines in the near plume spectrum. The copper impurities used for the diagnostic are from both the copper ignition wire and copper doping of the tungsten anode. Copper wire ignition, however, proved unreliable so an alternative method was used to determine the average capillary discharge plasma temperature.

The average plasma temperature between the capillary discharge electrodes can be approximated from the measured plasma resistivity. The plasma resistivity is more strongly dependent on the plasma temperature than on the number density over the temperature (0.75-1.5eV) and number density ($1x10^{23}$-$1x10^{25}$ m^{-3}) ranges typical for capillary discharges of this type as shown in Fig. 16. Figure 16 shows the calculated resistivity for an ablated polyethylene plasma as a function of plasma temperature for various electron number densities. It is fortuitous that the resistivity dependence on electron number density is the smallest at the average expected plasma temperature, 1eV.

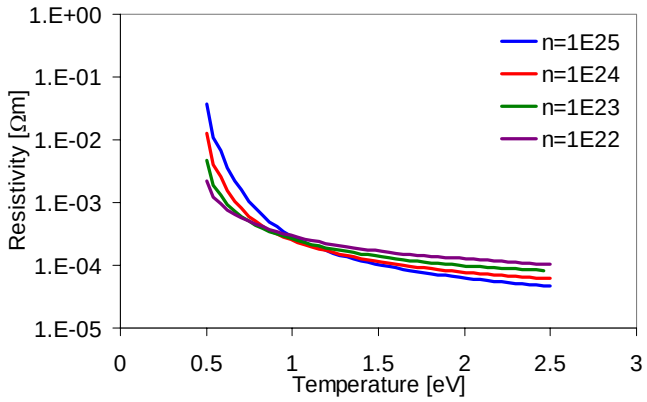

Figure 16. Polyethylene Plasma Resistivity.

Figure 17 shows the experimentally measured and model predicted resistance traces for various initial capacitor voltages. The experimental curves achieve approximately the same values as the model predictions, but the long tail extinction, again, causes a discrepancy. The plasma temperature during the discharge can be calculated by assuming an average number density, based on spectroscopic measurements, and using the curves from Fig. 16. Figure 18 shows the temperature traces estimated for the cases illustrated in Fig. 17.

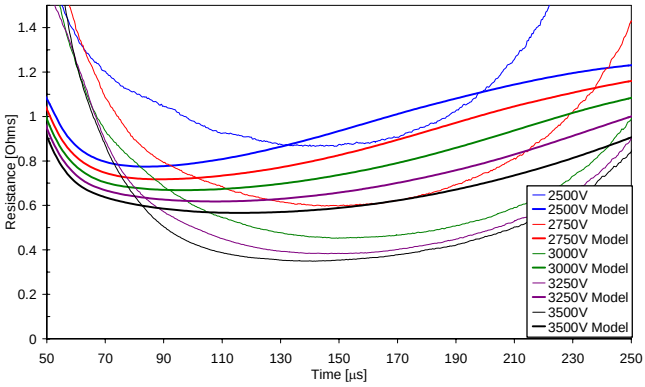

Figure 17. Capillary Discharge Resistivity.

The electron number density can be determined from measuring the broadening of the hydrogen Balmer alpha (H_a) spectral line.[19] In general the measured spectral line will be broadened due to natural broadening (~$1x10^{-5}$nm), Doppler broadening (<.1nm for these tests), Stark broadening (other pressure broadening terms are important if T<0.75eV), and diagnostic broadening (.1nm). For the conditions encountered in the capillary discharge experiment it is reasonable to consider only Stark broadening. For N_e in cm^{-3} units the full-width-half-max (in Angstroms) of the best fit Lorentzian for a Stark broadened hydrogen line is given by[20]

$$\Delta\lambda_{1/2}^{S,H} \cong 2.5x10^{-9}\alpha_{1/2}N_e^{2/3} \qquad (4)$$

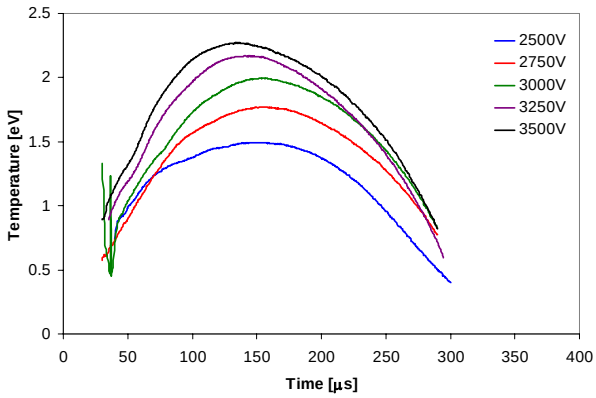

Figure 18. Capillary Discharge Temperature.

Although the best-fit Lorentzian for a Stark broadened hydrogen line profile does show a dependence on the plasma temperature through the fractional intensity width, $\alpha_{1/2}$, it is relatively small compared to the 2/3 power dependence of the electron number density that is shown in Fig. 19. An average temperature based on the results from the resistivity analysis was used for each case (1 eV was used for the $V_{cap,i}$ = 2500V case). Determining the electron number density using the Stark broadening analysis at plasma temperatures below approximately .75eV for a polyethylene sourced plasma with be inaccurate due to the importance of other pressure broadening mechanisms.

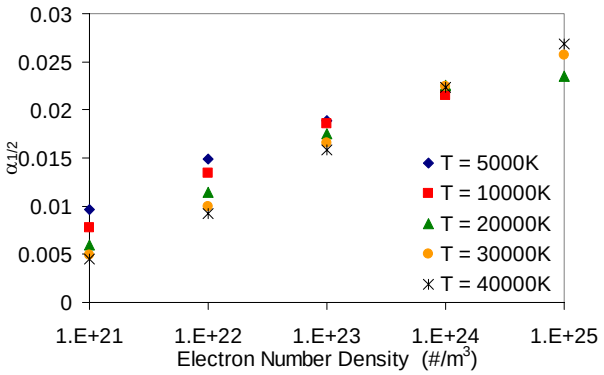

Figure 19. Hydrogen Fractional Intensity Widths.

Figure 20. shows a comparison of the electron number density profile determined from two separate experimental measurements, both with an initial capacitor voltage of 2500V, and the electron number density predicted from the model. The comparison is made for the electron number density at the cathode exhaust. The experimental uncertainty shown in Fig. 20 is primarily due to the uncertainty of the Lorentzian fit to the experimental data. Although all of the curves show the same general trend there is a significant difference (45%) in the peak height between experimental curves and the model predictions and additional work is required to determine the cause of the discrepancy.

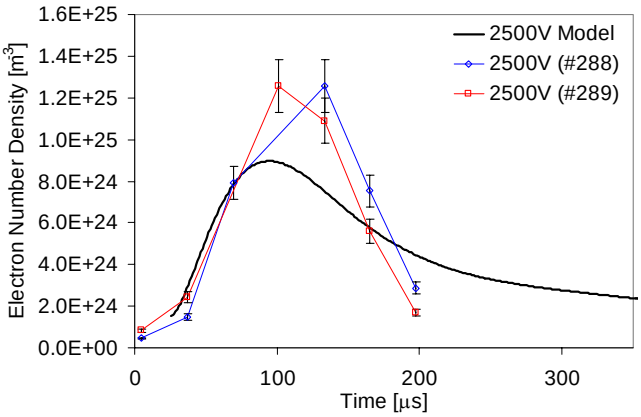

Figure 20. Electron Number Density Profile

IV. Capillary Discharge Thruster System

The agreement between the model predictions and the experimental results is typically within 20% indicating that the model is sufficiently accurate to make some approximate performance calculations for a capillary discharge based propulsion system. Such a propulsion system will require two major modifications to the current test configuration: a predictable, highly reliable multiple pulse ignition system and a continuous propellant feed system. This section will first make estimates of the possible performance levels of the capillary discharge based pulsed plasma thruster and then discuss what modifications to the capillary discharge will be required to make a thruster system.

A. Capillary Discharge PPT Performance Estimates

The validated capillary discharge model was used to make capillary discharge based PPT performance estimates. Fig. 21 shows the calculated thrust profiles for a variety of capillary discharge lengths and for the specific conditions of R_a=2mm, $V_{cap,i}$=3250V, C=5.5μF, Inductance=14μH. At a length of 2cm the thrust profile is symmetric, has a peak of 300N, and a pulse width of 275μs. As the length is increased from 2cm the peak height initially increases while the pulse width stays relatively constant. As the length is increased the number density during the pulse is increased which leads to the increased thrust. This increase is partly counteracted by a decrease in plasma temperature. A length of approximately 8cm corresponds to a maximum peak thrust level.

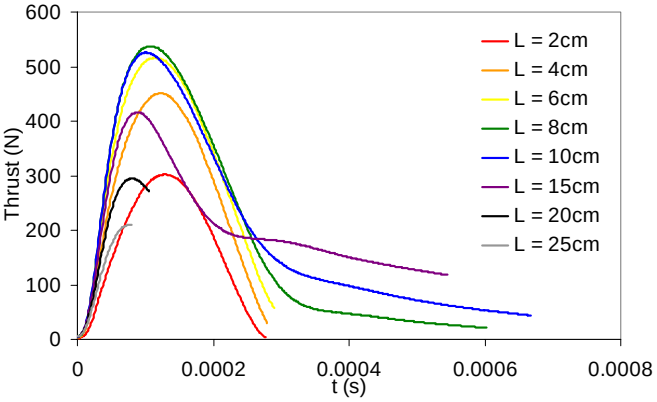

Figure 21. Thrust Profiles for Various Lengths.

Increasing the length beyond 8cm leads to decreased thrust levels for these specific conditions because the number density and temperature decrease due to decreases in the discharge current. The model encounters computational errors at lengths greater than approximately 20cm for these conditions and the discharge is not likely to be ignitable under those conditions.

Figure 22 shows the calculated specific impulse for the same conditions. At a length of 2cm a specific impulse of approximately 1150s can be achieved. Increasing the length of the capillary discharge corresponds to lower discharge currents and temperatures. The specific impulse decreases with increasing length and at lengths greater than 20cm the specific impulse is below 400s and is not of interest for spacecraft propulsion systems.

Figure 23 shows the calculated thrust profiles for various initial capacitor voltages. The model predicts that the minimum ignition voltage of 1750V is required to sustain the main discharge for a 10cm long capillary discharge. There is, however, some uncertainty in defining the low-voltage limit because of the simplicity of the present ignition model. At 1750V the thrust profile reaches a peak of 175N and is very asymmetrical with a long relatively intense extinction tail. As the initial capacitor voltage is increased the peak of the thrust profile increases due to the increased number density and temperature. The thrust profile also becomes more symmetric with the long extinction tail disappearing at the highest initial capacitor voltages.

Figure 24 shows the specific impulse as a function of the initial capacitor voltage. Increasing the initial capacitor voltage leads to an increase in discharge current and temperature throughout the discharge. The predicted specific impulse simply increases with initial capacitor voltage as expected. For a length of 10cm the specific impulse ranges between 600s and 850s for initial capacitor voltages

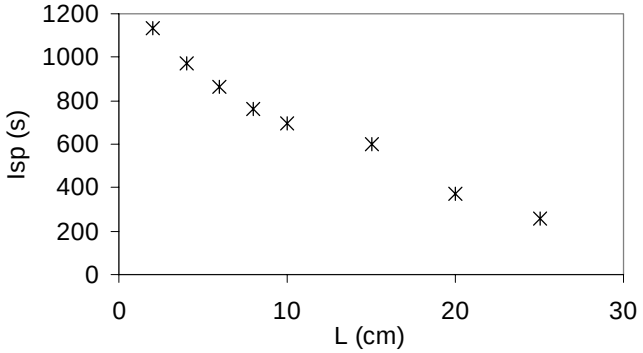

Figure 22. Capillary Discharge Specific Impulse for Various Lengths.

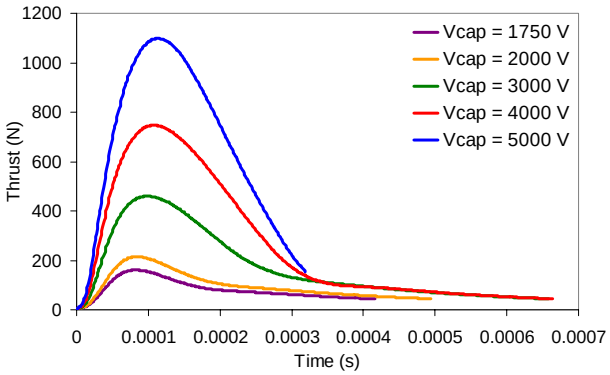

Figure 23. Capillary Discharge Thrust Profile for Various Initial Capacitor Voltages.

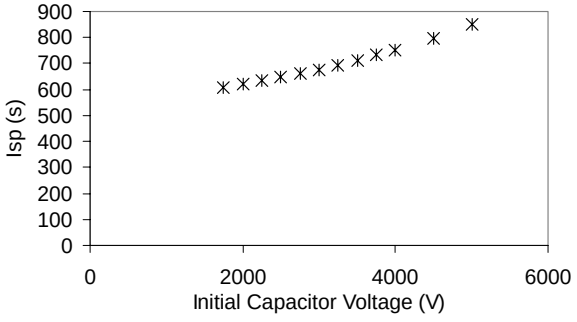

Figure 24. Capillary Discharge Specific Impulse for Various Initial Capacitor Voltages

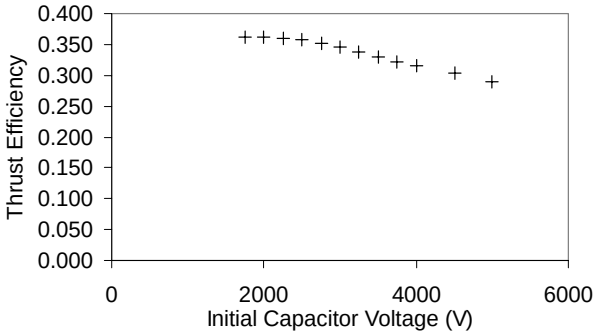

Figure 25. Capillary Discharge Thrust Efficiency for Various Initial Capacitor Voltages.

between 1750V and 5000V.

Figure 25 shows the calculated thrust efficiency as a function of the initial capacitor voltage. The thrust efficiency decreases with increasing initial capacitor voltage as a higher fraction of the energy is stored in internal modes as the temperature is increased. For this particular configuration the thrust efficiency ranges between 30% and 35%. Earlier work has indicated that thrust efficiencies in excess of 50% may be achievable with efficient nozzle expansion.[14] Only a limited number of specific performance calculations were made using the partially validated model, but it is clear, however, that the capillary discharge appears to have potential as a high-thrust, high-efficiency electrothermal PPT.

B. Capillary Discharge PPT Required Developments

The experimental and computational results indicate that a capillary discharge is an efficient source of high-density plasma and may have some applications as a high-power electrothermal PPT. Additional work must be completed to further understand its entire range of operation and to develop it into a thruster system. The potential of increased performance with nozzle expansion must be explored over the entire range of operation. There are two major design changes that are required to transform the current design into a thruster system: a predictable, highly reliable multiple pulse ignition system and a continuous propellant feed system. Alternative capillary discharge ignition systems such as segmented electrode ignition systems and spark ignition systems must be investigated. Segmented electrode ignition systems have been evaluated in the past and appear promising.[7] Alternative propellant feed systems such as multiphase propellant feed systems and high-pressure solid propellant feed systems must also be investigated.

V. Conclusion

Capillary discharges have been recently investigated as efficient pulsed sources of high-temperature, high-pressure plasmas. Although the focus for the development of high-pressure capillary discharges has historically been primarily for use in electrothermal-chemical guns, they may also find application in spacecraft propulsion systems. The investigation of capillary discharge based propulsion systems was begun by investigating the stereotypical capillary discharge. The basic operation of the capillary discharge was investigated using simple ignition and circuit models coupled with a 0D transient plasma model. The model was roughly validated from experimental results and indicated that the capillary discharge does indeed efficiently provide high-pressure plasmas. A series of experiments were completed and demonstrated the capillary discharge operation for various geometries, capacitor voltages, and LRC circuit inductances. Two distinct modes of operation were observed for capillary lengths below 10cm for the same nominal experimental conditions. Further investigation into the different modes of operation is required. Thruster calculations using the performance model indicate that the capillary discharge is an interesting pulsed plasma device even without efficient nozzle expansion. Future work must demonstrate alternative ignition systems, propellant feed systems, and efficient nozzle expansion.

References

1. Burton, R.L., and Turchi, P.J., "Pulsed Plasma Thruster," *Journal of Propulsion and Power*, Vol. 14, No. 5, 1998, pp. 716-735.
2. Kamhawi, H., Arrington, L., Pencil, E., and Haag, T., "Performance Evaluation of a High Energy Pulsed Plasma Thruster," AIAA 2005-3695, 2005.
3. Rysanek, F., and Burton, R., "Effects of Geometry and Energy on a Coaxial Pulsed Plasma Thruster," AIAA 2000-3429, 2000.
4. Edamitsu, T., and Tahara, H., "Performance Measurement and Flowfield Calculation of an Electrothermal Pulsed Plasma Thruster with a Propellant Feeding Mechanism," IEPC-2005-105, 2005.
5. Jahn, R.G., *Physics of Electric Propulsion*, Dover Publications, New York, 1996.
6. Benson, S.W., Arrington, L.A., Hoskins, W.A., and Meckel, N.J., "Development of a PPT for the EO-1 Spacecraft," AIAA-99-2276, 1999.
7. Zigler, A., Ehrlich, Y., Cohen, C., Krall, J., and Sprangle, P., "Optical Guiding of High-Intensity Laser Pulsed in a Long Plasma Channel Formed by a Slow Capillary Discharge," *J. Opt. Soc. Am. B*, 13, 1996, pp. 68-71.
8. Lee, R.W., and Zigler, A., "Multiple Pulse Laser Excitation of Capillary Discharge," *Applied Physics Letters*, Vol. 53, No. 21, 1998, pp. 2028-2029,
9. Powell, J. and Zielinski, A.E., "Theory and Experiment for an Ablating Capillary Discharge and Application to Electrothermal-Chemical Guns," Army Ballistic Research Laboratory, Report BRL-TR-3355, June 1992.
10. Zoler, D., Saphier, D., and Alimi R., "A Numerical Study of the Evolution of Plasma Parameters in an Ablative Capillary Discharge for a Two-Pulse Form of Energy Input," *J. Phys. D* , Vol. 27, 1994, pp.1423-1432.

[11] Zoler, D., and Alimi R., "A Proof of the Need for Consistent Treatment in Modeling of Capillary Ablative Discharges," *J. Phys. D*, Vol. 28, 1995, pp. 1141-1152.
[12] Gilligan, J., and Mohanti, R., "Time-Dependent Numerical Simulation of Ablation-Controlled Arcs," *IEEE Trans. Plasma Science*, Vol. 18, No. 2, 1990, pp. 190-197.
[13] Shafir, N., Zoler, D., Wald, S., and Shapira, M., "Reliable, Highly Reproducible Plasma Injectors for Electrothermal and Electrothermal-chemical Launchers," *IEEE Trans. Magn*., Vol. 41, No. 1, 2005, pp. 355-359.
[14] Pekker L., and Cambier J.-L., "A Model of Ablative Capillary Discharge," IHTC-13, Sydney Australia, August 13-18, 2006.
[15] Burton, R.L., Fleischer, D., Goldstein, S.A., and Tidman, D.A., "Experiments on a Repetitively Pulsed Electrothermal Thruster," *Journal of Propulsion and Power*, Vol. 6, No. 2, 1990, pp. 139-144.
[16] Burton, R.L., "Design and Predicted Performance of a Liquid Hydrogen PET Thruster," AIAA-88-3107.
[17] Prism Computational Sciences, Inc., 455 Science Drive, Suite 140, Madison, WI 53711.
[18] Taylor, M. "Formation of Plasma Around Wire Fragments Created by Electrically Exploded Copper Wire," *Journal of Physics D: Applied Physics*, 35, March 2002, pp. 700-709.
[19] Sueda, T., Katsuki, S., and Akiyama, H., "Early Phenomena of Capillary Discharges in Different Ambient Pressures," *IEEE Transactions on Magnetics*, Vol. 33, No. 1, January 1997, pp. 334-339.
[20] Griem, H.R., *Spectral Line Broadening by Plasmas*, Academic Press, New York and London, 1974.